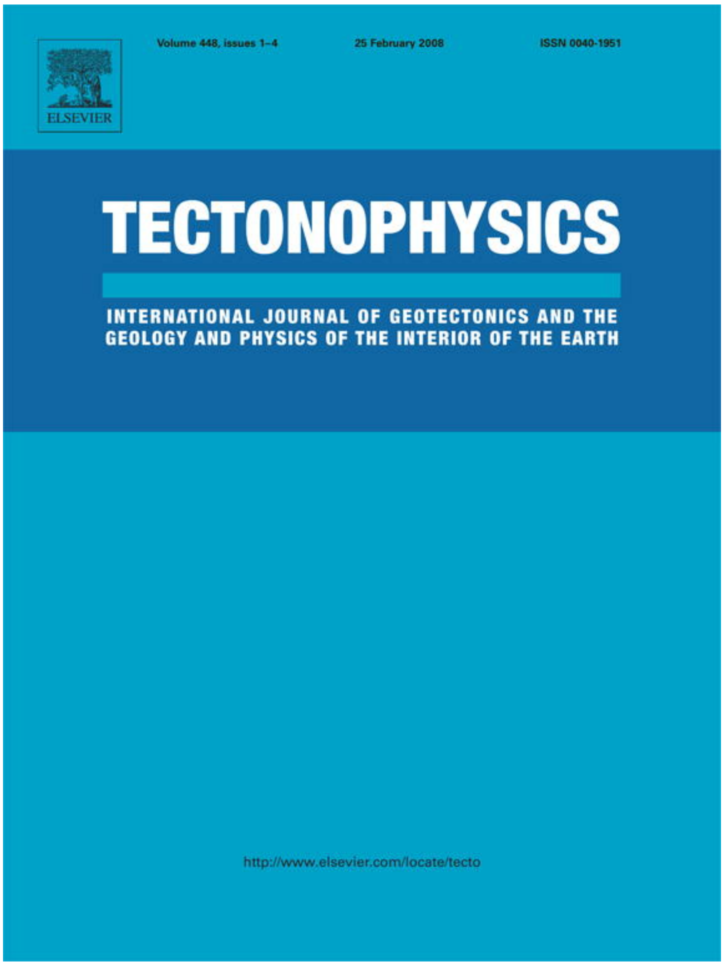
Volume 448, issues 1–4
25 February 2008
ISSN 0040-1951
ELSEVIER
TECTONOPHYSICS
INTERNATIONAL JOURNAL OF GEOTECTONICS AND THE GEOLOGY AND PHYSICS OF THE INTERIOR OF THE EARTH
http://www.elsevier.com/locate/tecto

ELSEVIER

Available online at www.sciencedirect.com
ScienceDirect

Tectonophysics 448 (2008) 20–32

TECTONOPHYSICS

www.elsevier.com/locate/tecto

3D seismic analysis of the Coast Shear Zone in SE Alaska and Western British Columbia: Broadside analysis of ACCRETE wide-angle data

Hongyan Li [a,*], Igor B. Morozov [a,b], Scott B. Smithson [a]

[a] University of Wyoming, United States
[b] University of Saskatchewan, Canada

Received 19 March 2006; received in revised form 1 August 2007; accepted 14 November 2007
Available online 21 November 2007

Abstract

The multidisciplinary ACCRETE project addresses the question of continental assemblage in southeast Alaska and western British Columbia by terrane accretion and magmatic addition. The previous studies of this project yielded important information for understanding the structures across the Coast Shear Zone (CSZ) and the formation of the CSZ and the Coast Mountains Batholith (CMB). The present study extends these interpretations into pseudo-3-D by using two additional wide-angle ACCRETE seismic lines. By analyzing the broadside wide-angle data using a series of laterally homogeneous 2-D models, we derive a lower-resolution 3-D velocity model of the outboard terranes and constrain variations in crustal thickness across and along the CSZ. Models of the broadside data confirms major structural and compositional trends extend along strike to the northwest. The key features are: a) a steep Moho ramp only ~15-km wide is coincident with the CSZ and divides thin (~25±1 km) crust to the west below the west-vergent thrust belt (WTB) from thicker (~31±1 km) crust to the east below the CMB, (b) low-velocity mantle (7.7–7.9 km/s) extends beneath the entire study region indicating high crustal and upper-mantle temperatures below the WTB and CMB, and (c) the Alexander terrane is characterized by strong mid-crustal reflectivity and high lower crustal velocities that are consistent with gabbroic composition. This study extends the earlier interpretation and implies that the ramp is indeed likely associated with transpressional tectonics and magmatic crustal addition east of the CSZ.

Keywords: Batholith; British Columbia; Crust; Coast Shear Zone; Coast Mountains; Moho; 3-D

1. Introduction

The accreted terranes and the continental arc in southeastern Alaska and western British Columbia represent one of the best areas to study the processes of continental crustal growth. During the Mesozoic and early Cenozoic, large-scale magmatism and terrane accretion took place as a result of oblique convergence between the Farallon and Kula plates and the North America plate (Chardon et al., 1999). This process led to the formation of one of the largest and most continuous magmatic arcs in the world, extending ~2000 km from the Southeastern Alaska and the Yukon to Northwestern British Columbia (Fig. 1). This Paleogene arc complex is referred to as Coast Plutonic Complex or Coast Mountain Batholith (CMB; the name used in this paper). This arc was formed by a combination of west-to-east stacking of the Insular (outboard) terranes to the Intermontane (inboard) terranes and accompanying magmatism (Crawford et al., 2000).

One of the outstanding tectonic problems of this area is the nature of the boundary between the Insular terranes consisting of the Alexander and Wrangellia terranes and the western margin of late Mesozoic North America, i.e., the Intermontane terranes (Rubin and Saleeby, 1992). Despite the advances in geological and geophysical studies, a controversy still remains about the nature of the accretion and the significance of the post-accretionary processes. Two unresolved questions are: locating the original accretionary front and determining the role

* Corresponding author. WesternGeco, 10001 Richmond, Houston, Texas, 77042, United States. Tel.: +1 713 468 1858(H), +1 713 689 7334(O); fax: +1 713 689 7475.
E-mail address: lhysnow@yahoo.com (H. Li).

0040-1951/$ - see front matter © 2007 Elsevier B.V. All rights reserved.
doi:10.1016/j.tecto.2007.11.009

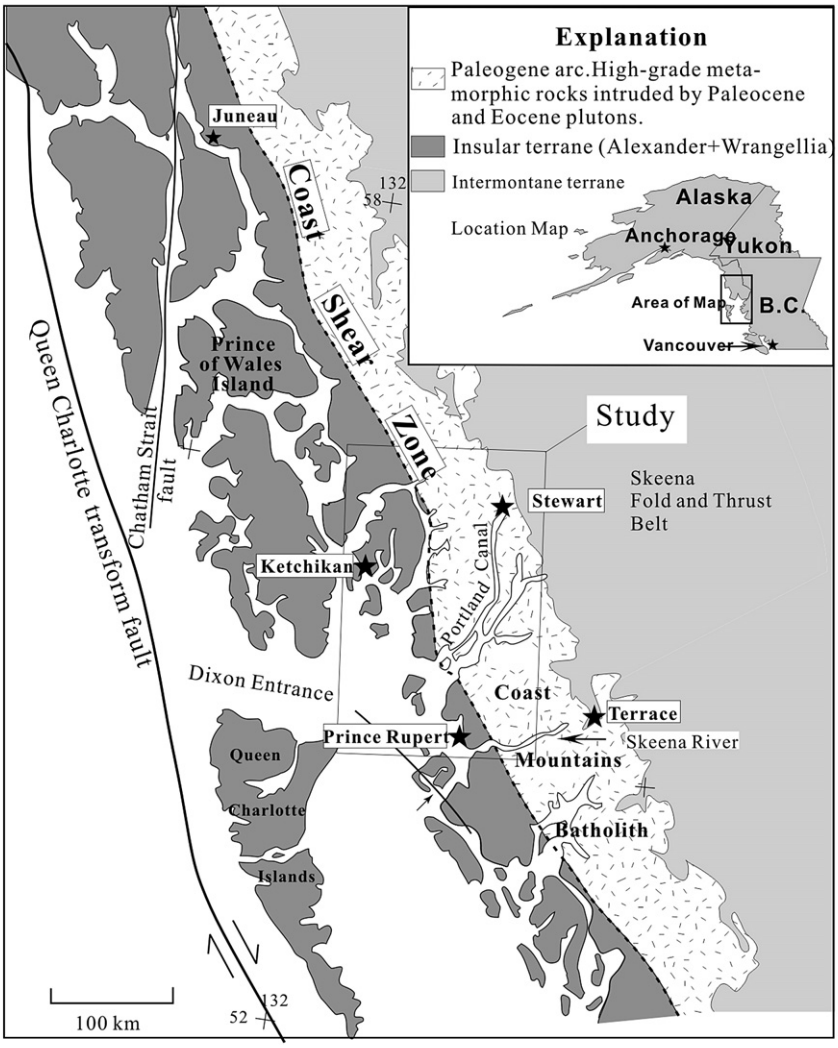

Fig. 1. Simplified terrane and assemblage map of southeastern Alaska and northwestern British Columbia (Morozov et al., 1998). The rectangle is the study area of ACCRETE project.

over time of the crustal-scale Coast Shear Zone (CSZ). From the previous seismic studies (Morozov et al., 1998, 2001, 2003), the CSZ marks the western boundary of the CMB and may truncate the thrust belt to the west. Based on the patterns of wide-angle seismic reflectivity, the CSZ was interpreted as subvertical through the crust separating terranes with different crustal thicknesses. The lower-crustal sections of these terranes exhibit strongly contrasting *S*-wave velocities suggesting a fundamental difference in their origins (Morozov et al., 2001, 2003).

Because of its cost, 3-D seismic reflection coverage of crustal structure is practically non-existent; yet, such coverage is extremely important to understand the behavior of structures in the third dimension. We take advantage of the flexibility of marine-land seismic recording suing marine-air guns from numerous ship tracks to obtain partial 3-D, wide-angle reflection coverage over the CSZ and are thus able to present a new, 3-D interpretation of the CSZ.

The interdisciplinary geological and geophysical project, ACCRETE, targeted the continental assemblage (Fig. 1) in the southeast Alaska and western British Columbia. The associated seismic study focused on the deep crustal structure, and particularly on elucidation of the crustal thickness across the CSZ (Fig. 1). The *P*-wave velocities beneath the CMB were interpreted in terms of its thermal and deformational processes, which might be manifested by the seismic velocity and reflection structure in the crust. In a broader framework, this study was incorporated with the overlapping Lithoprobe SNORCLE profiles that provided upper mantle velocity data and coverage across the eastern boundary of the CMB (Hammer et al., 2000).

In the previous analysis of ACCRETE data, 2-D wide-angle crustal *P*- and *S*-wave velocity models were derived for the main corridor following the Portland Canal fjord across the CSZ and CMB (Morozov et al., 1998, 2001), and the results were correlated with laboratory measurements using rock samples from the same area (Morozov et al., 2003). Marine-land acquisition in a fjord provided strong *P*–*S* wave conversion at the bottom of the fjord and resulted in well-constrained *P*- and *S*-wave velocity structures along the transect. The key findings of these studies leading to the present work were:

1) When corrected for high temperatures and erosion due to exhumation, the seismic properties under the CMB correspond

to those of the average continental crust (Morozov et al., 1998, 2001, 2003).

2) Magmatic addition was proposed as one of the main mechanisms of crustal growth (Morozov et al., 1998, 2001, 2003). Gabbro could have intruded a metasedimentary pile in the deep crust to cause crustal melting and then form intrusions of the CMB, leaving behind a mixture of mafic garnet granulite and sillmanite-garnet-quartz restite and generating the deeper part of what would become an average continental crustal section.
3) The Moho depth was found to be ~25 km west of the CSZ, with a ~15-km long ramp to ~31 km depth starting below the surface expression of the CSZ. This observation, together with disruption of the observed mid-crustal reflectivity, suggested that the CSZ could penetrate subvertically to nearly the total crustal depth (Morozov et al., 1998).

The objective of this paper is to utilize the ACCRETE broadside, fan-shot data generated by marine-air gun along extended ship tracks to test and extend the existing 2-D interpretations to three-dimensions (3-D). These data provide nearly continuous, albeit unreversed, coverage of the crust west of the primary ACCRETE corridor along Portland Canal and Dixon Entrance (Fig. 2). By analyzing the broadside wide-angle data using a series of laterally homogeneous 2-D models, we derive a lower-resolution 3-D velocity model of the outboard terranes and constrain variations in crustal thickness across and along the CSZ. Such results are seldom available in seismic crustal studies.

2. Tectonic and geologic setting

The study area crosses the outer Insular terranes into the CMB plutonic suture generated by the accretion of the Insular terranes to the Intermontane terranes (Fig. 1). This area provides a link across the boundary between the Insular terranes and the Intermontane terranes because it is relatively unaffected by Tertiary plutonism (Rubin and Saleeby, 1992).

The CMB is one of the world's largest intrusive complexes and represent the suture zone of the last North American accretion episode. The batholith experienced a two-phase evolution (Klepeis et al., 1998; McClelland et al., 2000), initially formed by subduction and then collision of accreted terranes during plate convergence, and followed by Paleocene and Eocene exhumation during a transition from a dominantly compressional regime to extension or transtension (Klepeis et al., 1998; McClelland et al., 2000). The CMB consists of three northwest-trending belts of calc-alkaline batholiths from

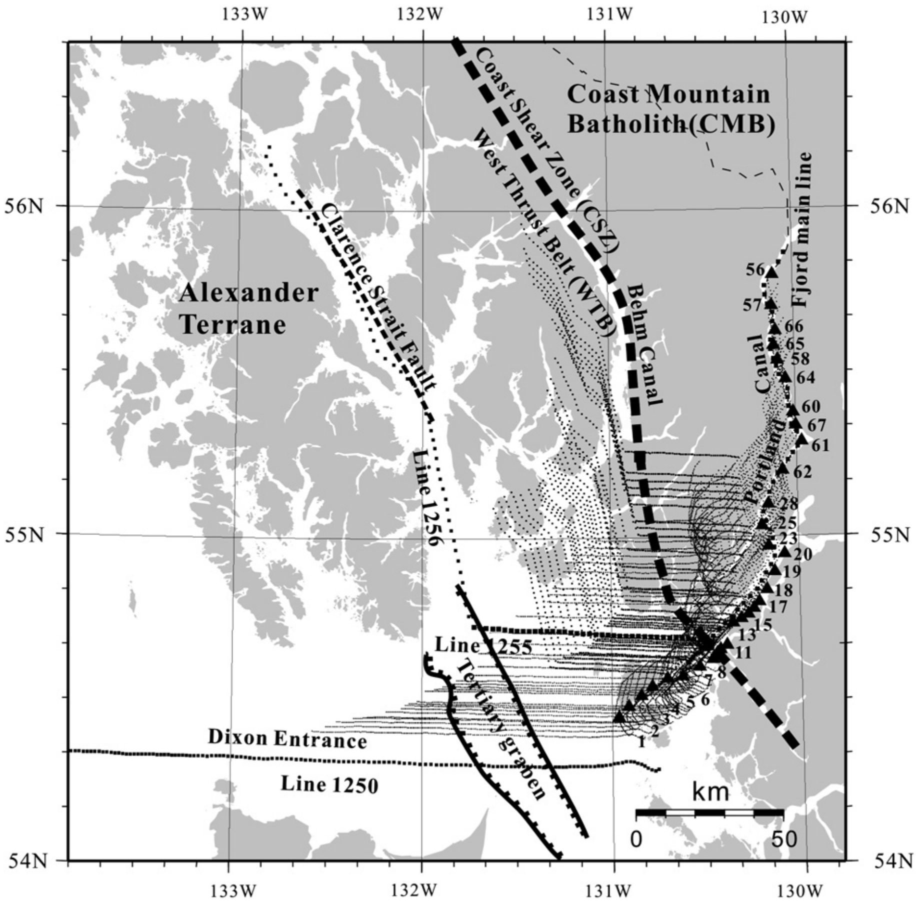

Fig. 2. Location map of the ACCRETE wide-angle experiment area discussed in this paper. Triangles indicate REFTEK recording stations with station numbers. Larger black dots are shot lines 1255, 1256, 1250, and the 2-D Portland Canal line; the smaller black dots are the midpoints from these lines. The thick dashed line is the Coast Shear Zone (CSZ). A Tertiary graben (Rohr and Currie, 1997) is also shown.

northwest to southeast: 1) a Jurassic belt; 2) early- to mid-Cretaceous batholiths; 3) a voluminous Eocene belt (Chardon et al., 1999).

To the west of the CMB within the Insular terranes, the rocks mainly consist of Paleozoic metavolcanic rocks and clastic metasedimentary rocks as well as upper Jurassic and lower Cretaceous metamorphosed volcanic rocks and turbidite sequences. In the study area, the metamorphic grade increases eastward from lower greenschist facies to upper amphibolite facies (Crawford and Hollister, 1982; Rubin and Saleeby, 1992). Broadly coeval with arc magmatism, mid-Cretaceous west-vergent thrusting occurred along parts of the eastern boundary of the Alexander terrane, leading to an imbricate series of a west-vergent thrust belt or WTB (Rubin and Saleeby, 1992).

The Coast Shear Zone (CSZ) divides the Insular terranes from the CMB (Fig. 1), and corresponds to the western Paleogene magmatic front of the Cordillera (Van Der Heyden, 1992; Hollister and Andronicos, 1997). It is a prominent structure of the central Coast Mountains orogen forming a band of intense deformation 2–6 km wide and extending for 800 km along strike (Klepeis et al., 1998; Crawford et al., 2000). West of the CSZ, westward thrusting, pluton emplacement, high-pressure metamorphism, and subsequent regional cooling occurred between 100 and 80 Ma; while on the east of the CSZ, most of the plutonism and regional cooling occurred between 60 and 48 Ma (Crawford et al., 1987).

3. Seismic dataset

The wide-angle reflection-refraction data used in this study are parts of a larger seismic data set collected in September 1994 by the ACCRETE project (Morozov et al., 1998, 2001), partly overlapping with Lithoprobe SNORCLE corridor (Hammer et al., 2000; Hammer and Clowes, 2004). The present study focuses on ACCRETE lines 1255 and 1256 that were not included in the previous investigations (Fig. 2). Line 1255, with ~50-m air gun shot spacing, extends for ~80 km west from the CSZ to one of the Tertiary grabens in the Dixon Entrance (Fig. 2; Rohr and Currie, 1997; Morozov et al., 2001). Line 1256 (with ~100-m shot spacing) is nearly parallel to the CSZ and extends northward along the Clarence Strait for ~150 km (Fig. 2). REFTEK digital seismic recorders were deployed on land at 3–5 km spacings along the Portland Canal fjord (Fig. 2). Note that stations 8, 9, 10, and 11 (Fig. 2) were placed relatively closely together (<2.5 km apart) and almost inline with line 1255, which provided a good geometry to constrain the velocity structure to the west of the CSZ. As with other ACCRETE wide-angle data (Morozov et al., 1998), the data quality from lines 1255 and 1256 was generally excellent.

Due to the unique seismic acquisition in fjords, the primary refraction and reflection phases are strong and consistent but the reverberatory nature of the fjord data (due to the reflections from the narrow fjord walls, from the P/SV mode conversions, etc; Morozov and Din, in press) makes the secondary arrivals somewhat emergent in character, particularly at further offsets.

4. Data processing and inversion

The broadside source-receiver geometry of this study resulted in a limited 3-D interpretation. Since the distribution of midpoints from line 1255 crosses the CSZ (Fig. 2), this source line is particularly important for our study. Because of the unreversed 3-D ray coverage, we adopted a simplified interpretation scheme, based on iterative 2-D modeling of the travel times from groups of adjacent stations. Nine such groups were assigned based on station proximity and travel-time similarities; these groups combine station numbers 1–3, 4–7, 8–11, 13–14, 16–19, 20–28, 61–60, 64–66, and 57–56 (Fig. 2). Because of the unreversed coverage, the inverted 2-D

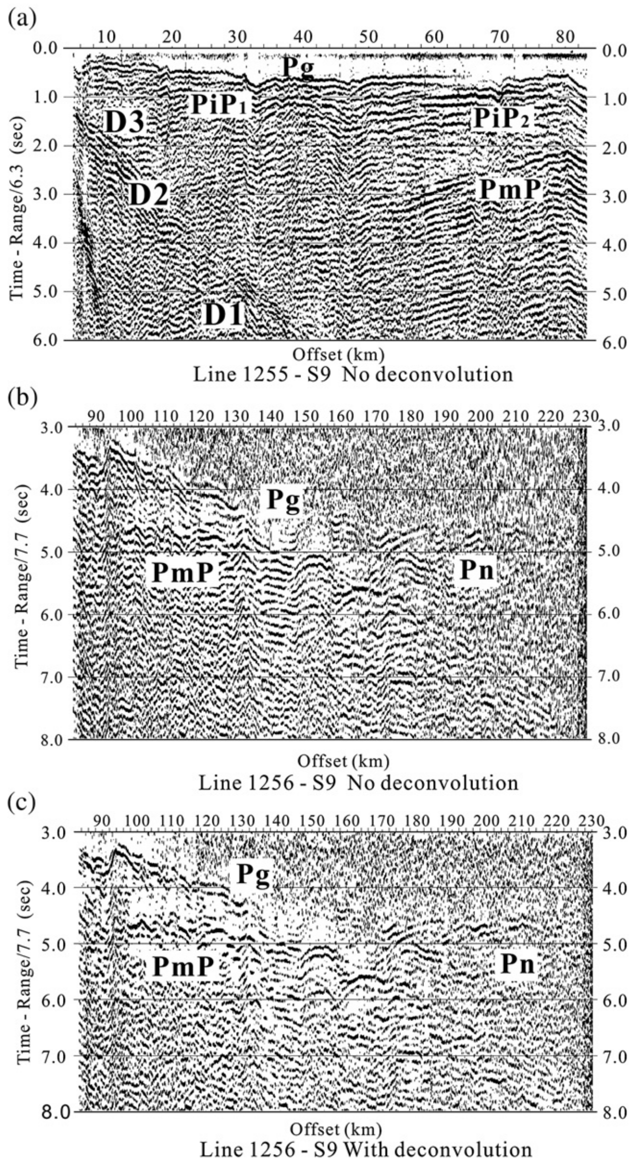

Fig. 3. Water-depth corrected vertical-component receiver gather of station 9; (a) from line 1255; (b) from line 1256; (c) from line 1256 after minimum phase predictive deconvolution, with operator length of 500 ms and prediction distance 140 ms. *Pg*, *Pn*, crustal reflections PiP_1 and PiP_2, and Moho reflections are observed. Labels D1, D2, and D3 indicate dipping reflections in (a) which could correspond to the thrust faults determined by Morozov et al. (1998, 2001). Compared to (b), the effect of ringing is highly reduced after deconvolution (c).

structures for each group had to be kept "minimal" in the sense of being as close to 2-D horizontally layered models as possible. Continuity with the interpretation of the reversed Portland Canal line (Fig. 2; Morozov et al., 1998, 2001) was another critical constraint on the interpretation. After all nine 2-D models were built in a consistent manner, they were combined to create a 3-D view.

The following groups of arrivals were observed and used in this study: 1) upper-crustal refractions and reflections (*Pg* and *PiP*1, Fig. 3) to determine the upper crustal velocity and thickness, 2) intracrustal reflections (*Pg* and *PiP*2, Fig. 3) to constrain the mid-crustal velocities and depths, 3) Moho reflections (*PmP*, Fig. 3) to determine the crustal thickness and the lower crustal velocities, 4) upper-mantle refractions to constrain the upper mantle velocity and give additional constraints on the crustal thickness (*Pn*, Fig. 3).

4.1. Phase Identification

Due to the acquisition in fjord the wavelet is somewhat ringy (Fig. 3) with dominant frequencies between 6–8 Hz. By comparing the spectra of the pre-phase noise and the useful phases, the noise (mostly waves and wind) was found to be mainly concentrated at frequencies below 5 Hz.

Prior to travel-time picking, bandpass filtering and AGC were applied to enhance the arrivals. For different stations, the available offset ranges varied (Fig. 2), leading to different filtering frequency bands selected for optimal phase identification and picking. For the near-offset stations, the frequency pass bands were 2–4–10–15 Hz (Fig. 3a), and at farther offsets, a 2–4–8–10 Hz filter was used (Fig. 3b). Secondary phases were contaminated by strong reverberations (Fig. 3b), which made their picking more difficult. By using minimum-phase predictive deconvolution, the ringy effect was highly minimized (Fig. 3c), especially for line 1256. In order to improve the credibility and consistency of picking, travel-time picks were made from deconvolved records and compared to those from the raw sections.

Phase correlation of crustal arrivals from both lines 1255 and 1256 was accomplished by comparing the adjacent receiver gathers and repeated checks for picking consistency. Due to the 3-D nature of the experiment, seismic waves recorded by adjacent instruments may not have followed the same travel paths. However, these paths should be similar, especially for the more distant stations (Fig. 2), and therefore, the picks from adjacent stations should vary in a systematic manner, which was observed within the selected station groups.

4.1.1. Line 1255 arrivals

The upper crust is defined by refractions and an upper crustal reflection phase. The nearest available offset was 5 km from station 9. The first arrivals on the closer stations (1–28) exhibit two distinct groups of moveouts of 5.9–6.0 km/s and 6.2–6.3 km/s (Fig. 3a) suggesting a two-layer, upper-crustal structure. The first arrivals on the far stations from 62 to 56 also have moveouts suggesting a velocity of 6.2–6.3 km/s. The picking errors (Table 1) range from 20 to 40 ms, generally increasing with increasing offset. Moreover, a clear upper-crustal reflection phase (P_iP_1; Figs. 3a and 8b, picking error ~30 ms) is observed on stations 1-14.

A mid-crustal boundary producing a strong reflection at offsets of ~40-90 km is widely observed (labeled PiP_2 in Fig. 3a) from all the stations 1 to 28, but no refractions corresponding to this boundary were found in line 1255 due to the limited offsets.

Similarly to the Portland Canal records (Morozov et al., 1998), most Moho reflections (Figs. 3a and 8b) are consistently strong in this area and are observed clearly on all seismic stations. From stations 1 to 28, Moho reflections were observed at offsets from ~50 to 108 km, and from stations 62 to 56 — at offsets from 70 to 140 km.

4.1.2. Line 1256 arrivals

Most of the first arrivals on stations 1 to 14 with offset <140 km (*Pg*) were clear and the pick error can be as less as 40 ms by comparing the picks from adjacent shots and adjacent stations. The first arrivals were not picked for other far stations due to the data quality. The velocities of the observed crustal refractions on line 1256 are ~6.2–6.3 km/s and ~6.4–6.5 km/s (Figs. 3, 5 and 8).

The *Pn* phases were observed between offsets of 140 to 220 km, which are clear on stations 1 to 10 and some farther

Table 1
Velocity structure SW of the Western Thrust Belt (WTB)

ACCRETE station Numbers (Fig. 2)	Layer 1			Layer 2			Layer 3			Layer 4			Pn
	Vel km/s	Time Error ms	Depth. km	Vel km/s	Time Error ms	Depth. km	Vel km/s	Time Error ms	Depth. km	Vel km/s	Time Error ms	Depth. km	Vel km/s
1,2,3	5.9–6.0	±40	3.3–3.7	6.2–6.3	±40	7.6–8.4	6.4–6.5	±40	11–12.5	6.6–6.8	±30	24.0–26.0	7.7–7.9
4,5,6,7	5.9–6.0	±30	3.3–3.7	6.2–6.3	±20	7.7–8.3	6.4–6.5	±30	11.0–12.0	6.6–6.8	±40	24.5–26.0	7.7–7.9
8,9,10,11	5.9–6.0	±20	3.4–3.6	6.2–6.3	±20	7.8–8.2	6.4–6.5	±20	11.2–11.8	6.6–6.8	±30	24.5–25.5	7.7–7.9
13,14	5.9–6.0	±20	3.4–3.6	6.2–6.3	±25	7.8–8.2	6.4–6.5	±30	11.0–12.0	6.6–6.8	±40	24.5–25.5	7.7–7.9
16,17,18,19	5.9–6.0	±40	3.3–3.7	6.2–6.3	±30	7.6–8.4	6.4–6.5	±40	12.4–13.6	6.6–6.8	±40	24.5–26.5	
20,23,25,28				6.2–6.3	±30	7.6–8.4	6.4–6.5	±40	13.4–14.6	6.6–6.8	±40	25.0–27.0	
61,67,60										6.6–6.8	±100	25.0–28.0	7.7–7.9
64,58,65,66										6.6–6.8	±100	25.0–28.0	7.7–7.9

The velocities of the WTB are calculated according to the refractions picked along line 1255 and 1256 (Fig. 5). The velocity of layer 4 is determined by Moho reflection modeling combined with the previous study (Morozov et al., 2001). The depths of the layers are obtained by travel-time modeling (Zelt and Smith, 1992).

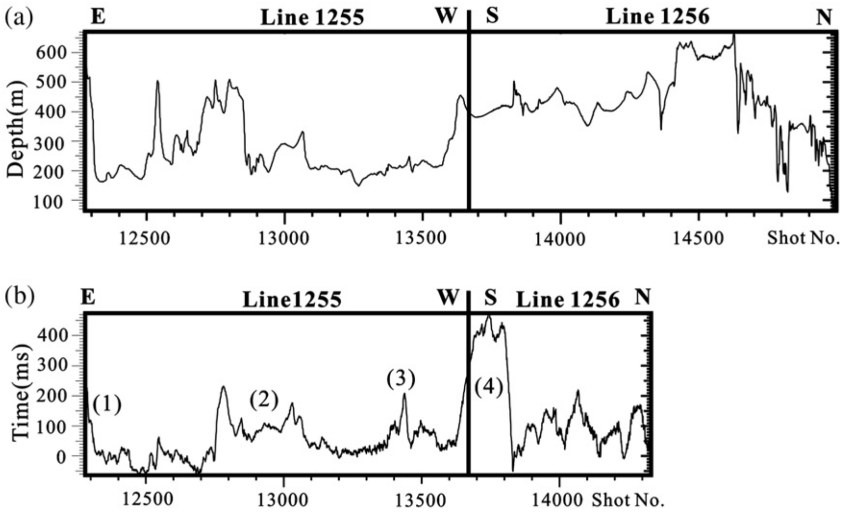

Fig. 4. Water depth (a) and shot statics for shot line 1255 and 1256. The water depth varies from ~100 m to ~650 m. These shot statics are computed from the first arrival picks of stations 7, 8, 9, 10, 11, 13, and 14. Note four areas with abnormally high shot statics in line 1255 (labeled). The largest shot statics (4) corresponds to a Tertiary graben (Fig. 2). Because of insufficient data, the shot statics were not considered for the shots of line 1256 further north, zero shot statics are assumed.

stations (61, 64, 58, 65, 66, and 57) with weak amplitudes. The velocity of *Pn* is determined as ~7.7–7.9 km/s (Figs. 3b, 5 and 8).

Moho reflections are observed quite well on all the stations of line 1256 at offsets of up to 160 km, but the picking accuracy decreases with offset. Occasional cycle skipping could also lead to ~140 ms travel-time errors (Figs. 3 and 8). Picking error was reduced by comparing the Moho reflections from line 1255 with the same station and from adjacent stations.

4.2. Statics corrections

Strong water-depth variations (Fig. 4a) lead to significant statics complicating the interpretation in our approach based on horizontal 2-D or minimum-structure 2-D inversion. To reduce these statics, the water depth effects were first removed from the travel-time picks by using a velocity replacement:

$$T_{\text{wstat}} = T_{\text{pick}} - \left(\frac{D_w}{v_w} - \frac{D_w}{v_s}\right)$$

where, T_{wstat} is the corrected travel time in ms; T_{pick} is the picked time; D_{w} is the water depth from multichannel reflection data; and v_{w} and v_{s} are the acoustic velocities in water (1.5 km/s) and in the basement rock (5.5 km/s; Clowes and Gens-Lenartowicz, 1985; Yuan and Spence, 1992; Morozov et al., 1998).

After removal of the water depth effects, the first-arrival picks from different stations showed similar offset-time trends (Fig. 5a) yet still exhibited strong variations correlated with shot and receiver positions (Fig. 5b). These statics are caused by the

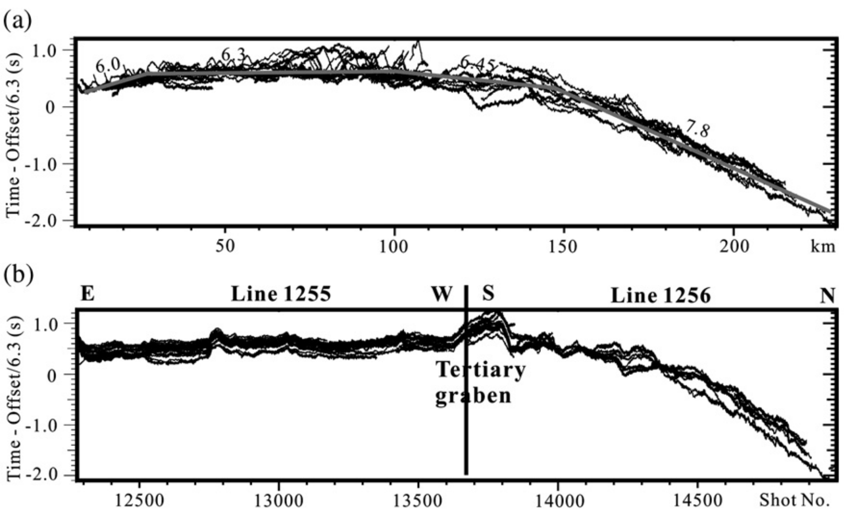

Fig. 5. First-arrival picks from stations 1–28 of shot lines 1255 and 1256 at different offsets (a) and with corresponding shot numbers (b). Solid grey line in (a) indicates the four different moveouts constrained from the observed travel-times: 6.0, 6.3, 6.45, and 7.8 km/s, according to the trends of the first-arrival picks. The anomalous picks between offset 50 and 90 km correspond to the Tertiary graben (Fig. 2).

variations of the sedimentary thickness beneath the shot lines, similar to those observed by Morozov et al. (1998). The largest statics of ~300–400 ms were found near the western end of line 1255 and the southern end of line 1256 due to the Tertiary graben. Because the nearest shot-receiver offset was ~5 km, shallow velocities could not be determined from the data, and the thickness of the sediments was constrained from the intercept times of the first observed refractions by assuming a constant velocity of 3.0 km/s (Chen, 1998; Yuan and Spence, 1992) within the sediments. The distribution of the midpoints of all the first arrival picks (*Pg* and *Pn*) is shown in Fig. 6a.

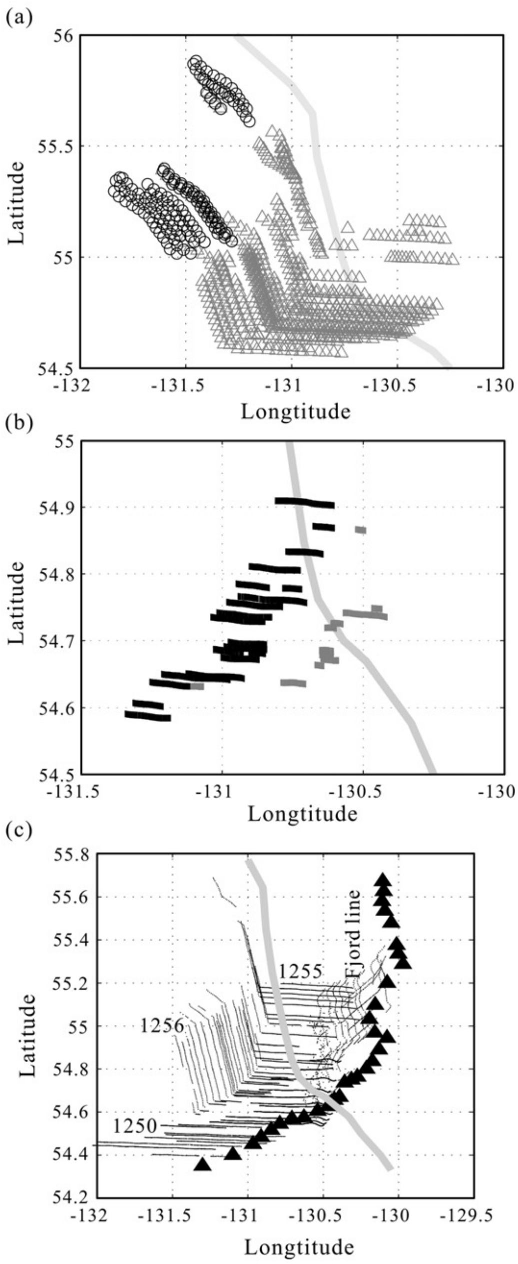

Fig. 6. The midpoint distribution of all the picked phases, (a) First arrivals, *Pg* (grey triangles) and *Pn* (black circles); (b) Upper crustal reflections PiP_1 (grey lines) and mid-crustal reflections PiP_2 (black lines); (c) Moho reflections from line 1255, 1256, 1250 and 2-D fjord line (Fig. 2). The grey thick line shows the location of the CSZ.

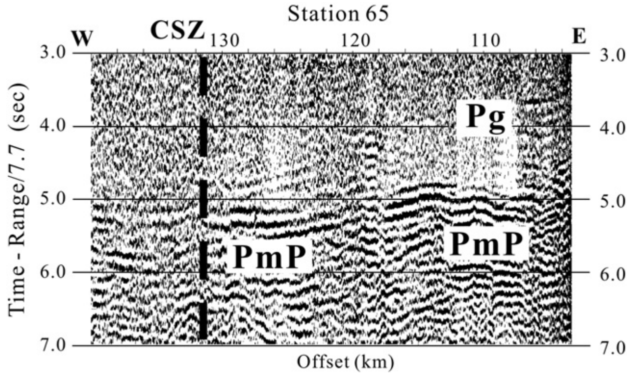

Fig. 7. Vertical-component receiver gather 65 from line 1255 with reduction velocity 7.7 km/s after both water-depth and shot-static corrections. The phases become much smoother and easier to pick consistently. It is also clear that the Moho is dipping to the east.

Four distinct linear moveouts were identified in the first-arrival picks (6.0 km/s, 6.3 km/s, 6.45 km/s, and 7.8 km/s; Fig. 5a), and the corresponding velocities were used to construct our models. By using a generalized time-term method (Chen, 1998; Morozov et al., 1998), shot statics (Fig. 4b) along line 1255 and 1256 and the receiver statics were determined. The shot statics at the north part of line 1256 was not calculated because few first arrivals were observed within this far offset range and the data quality is low. No reflections from this shot segment were used in this study. After the static corrections are applied, the refractions and reflections became much smoother, and picking the secondary arrivals from receiver gathers became easier and more reliable (Figs. 7 and 8).

4.3. Travel-time inversion

After grouping the stations into nine groups, the travel times were inverted using interactive 2-D ray tracing (Zelt and Smith, 1992). The inversion started from stations 8–11, which are almost in line with line 1255 (Fig. 2). Since stations 8–11 are very close to each other (Fig. 2), horizontal layering was assumed in this area. By fitting the traveltimes from the first arrivals and reflections, a five-layer velocity model was obtained (Fig. 8): low-velocity (5.0–5.5 km/s) to the depth of ~0.8 km, two upper crustal layers, 5.9–6.0 km/s to ~3.5 km, 6.2–6.3 km/s to the depth of ~7 km, and one mid-crustal layer, 6.4–6.5 km/s to the depth of ~12 km, and the lower crust of 6.6–6.8 km/s, with a Moho depth of ~26 km. The lower-crustal velocity and Moho depth were constrained from Moho reflections and *Pn* refractions, consistent with the previous results (Morozov et al., 1998, 2001). The velocity within the uppermost mantle was determined as 7.7–7.9 km/s. The initial 2-D, 5-layer model was then applied to generate 5 other 2-D models using data picked from 5 other groups of stations (13–14, 16–19, 20–28, 5–7, and 1–4; Fig. 2). Due to lack of 3-D sampling, layer velocities were held constant and the travel-time inversion was allowed to fit layer thickness within pick error bounds. With layer thickness adjustments of <2 km, the initial five-layer model was also found to fit the observations from other station groups. The crustal velocity models determined from 2-D ray-

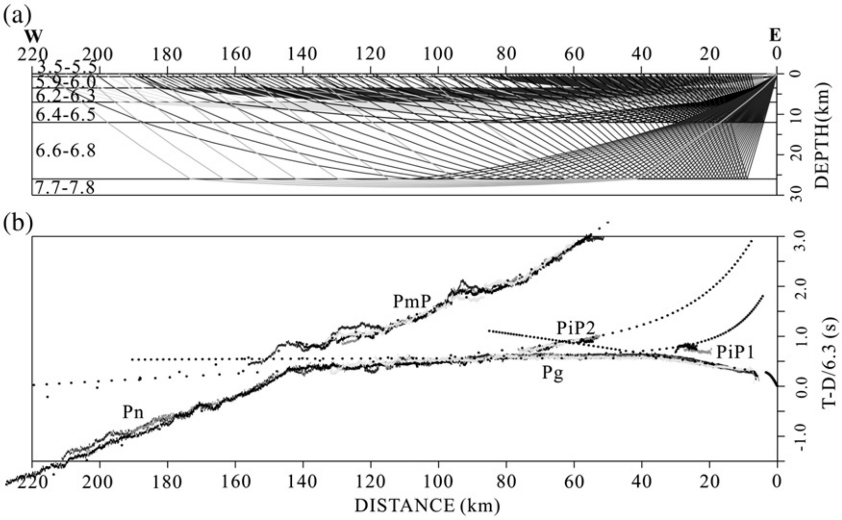

Fig. 8. *P*-wave velocity model constrained from the refraction and reflection picks at stations 8, 9, 10, and 11 from shot lines 1255 and 1256; (a) Ray diagram and the velocity model; (b) comparison of the observed (after static corrections, solid lines) and modeled (dots) traveltimes. Velocity values in km/s are labeled in plot (a). The different colors from light to dark grey represent stations 11, 9, 8, 10 respectively.

tracing modeling are summarized in Table 1. The distribution of the midpoints of all the crustal reflections is shown is Fig. 6b, and all the Moho reflection picks are shown in Fig. 6c.

Because Moho reflections are strong within the entire shot line 1255, and their mid-points cross the CSZ (Figs. 2 and 6c), observations from the far-offset stations 62–56 (Fig. 7) are essential for constraining the variations of the Moho depth across the CSZ. Due to greater offsets, the upper crustal velocity information was not available for these far stations. However, the upper crustal velocity models determined from station groups at near offsets (Table 1) do not change much with station locations. Furthermore, the velocity models along the Portland Canal 2-D profiles (Morozov et al., 1998; Hammer et al., 2000) exhibit laterally consistent upper crustal velocity models. Therefore, we used the upper-crustal velocity model from the adjacent group of stations 20–28 for modeling the travel times from stations 62–56 at farther offsets. The Moho reflections from these far stations (Fig. 7) clearly demonstrate a dipping Moho toward the east. Through 2-D ray tracing, the Moho reflections recorded on farther stations fit the velocity model across the CSZ determined from the 2-D fjord line (Morozov et al., 1998, 2001). The Moho depth is ~26.5 ± 1.5 km to the west and up to ~31 ± 1.5 km to the east of the CSZ (Fig. 9). The consistent misfit of both *Pg* and *PmP* at the far offset could be due to the shot statics along line 1256. The *Pn* refractions are clear for some of the far-offset stations (Fig. 6a), and the observed *Pn* velocity is similar to those obtained from the southern stations, 7.7–7.9 km/s, also in agreement with the previous studies (Morozov et al., 1998; Hammer et al., 2000; Morozov et al., 2001; Hammer and Clowes, 2004).

4.4. 3-D depth/velocity model

Due to a scattered midpoint coverage (Fig. 2), cross-sections resulting from the individual station groups can be combined into a composite 3-D model. The crust of the WTB is modelled with four crustal layers beneath a low-velocity sedimentary cover of 0.4–0.8 km thickness. Note that the sedimentary cover is primarily constrained by stations 1–19 and may also be influenced by the shot or station statics due to the limited near-offset coverage by the broadside dataset. The four crustal layers are: two distinct upper crustal layers (5.9–6.0 km/s to the depth of ~3.3–3.7 km and 6.2–6.3 km/s to ~7.5–8.5-km depths), a middle crustal layer with velocities of 6.4–6.5 km/s to ~11–14-km depths, and a 6.6–6.8-km/s lower crustal layer to the depth of ~24–27 km (Table 1).

Refraction velocities and travel-time delays provide information about the sediment thickness and Tertiary grabben structure cross-cut by the profiles. Stations 1–28 (Figs. 4b and 5) indicate thickening of the sediments near ~80 km west of the CSZ, corresponding to a Tertiary graben (Fig. 2; Rohr and Currie, 1997). In addition, increased sedimentary thickness is observed close to the CSZ (location (1) in Fig. 4b) and near the surface projections of the interpreted WTB thrust faults. The locations (2) and (3) in Fig. 4b may correspond to the thrust faults W2 and W3 in Fig. 10. Similar observations were made by Morozov et al. (1998, 2001). The reason for such delays could be complex velocity structure associated with the fault zone.

The pseudo-3D crustal model provides coverage to the west of the initial ACCRETE corridor along the Portland Canal, adding along-strike constraints of crustal thickness across the CSZ. The midpoints of the picked Moho reflections covered ~100 km from west to east and ~90 km from south to north, providing good coverage across the WTB, CSZ, and below the CMB (Fig. 6c).

In order to measure the resulting errors in crustal velocities and Moho depths, let us denote *t* the modeled Moho reflection time, *z* — Moho depth, *V* — crustal velocity, and *x* — the source receiver offset. By taking the logarithm of the hyperbolic moveout equation:

$$\log t = \log \sqrt{(x^2+z^2)/V^2} = \frac{1}{2}\log\left(x^2+z^2\right) - \log V, \qquad (1)$$

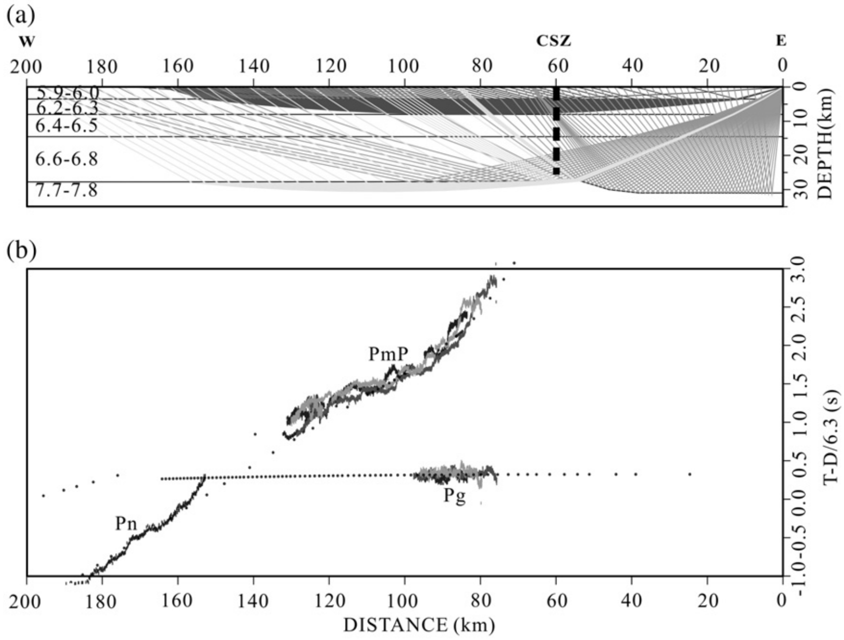

Fig. 9. *P*-wave velocity model constrained from the refraction and reflection picks from stations 61, 67, and 60 using shot lines 1255 and 1256. All static corrections were applied to the picks. The upper crustal velocity structure was taken from the results of stations 20–28 because no upper crustal information is available for these stations. The different colors from light to dark grey represent stations 67, 61, and 60 respectively.

the relative deviation in t due to variations in V and z can be estimated as:

$$\frac{\Delta t}{t} \approx \frac{z\Delta z}{x^2+z^2} - \frac{\Delta V}{V} \approx \left(\frac{z}{x}\right)^2 \frac{\Delta z}{z} - \frac{\Delta V}{V} \tag{2}$$

because $x \gg z$ for the wide-angle data. Thus, the estimated standard travel-time variance is:

$$\left\langle \left(\frac{\Delta t^2}{t}\right)^2 \right\rangle \approx \left(\frac{z}{x}\right)^4 \left\langle \left(\frac{\Delta z}{z}\right)^2 \right\rangle + \left\langle \left(\frac{\Delta V}{V}\right)^2 \right\rangle. \tag{3}$$

Therefore, errors in the velocity affect the modeled Moho reflection time much stronger than depth errors. Due to limited control on crustal velocity in large portions of the study area, we tested different average crustal velocities in order to minimize the error between the picked and modeled PmP arrivals. By fitting the Moho reflection picks from lines 1250, 1255, and part of 1256 with midpoints located to the west of the CSZ, the error between the picked and the modeled Moho reflection time was found the smallest when using an average crustal velocity of 6.44 km/s and with a depth of 25 km below the WTB (Fig. 11a, b). With an average velocity of 6.44 km/s, some of the Moho picks from line 1255 (Fig. 11c) and the main fjord line (Fig. 11e) were aligned, and the anomalies in both figures correspond to the picks with midpoints located within the CMB, where the Moho is deeper (indicated by black boxes in Fig. 11). By applying an average velocity of 6.55 km/s (Morozov et al., 1998) with Moho depths of 28 and 30 km respectively to the Moho picks from line 1255 (Fig. 11d) and the main fjord line (Fig. 11f), the anomalies with large errors in Fig. 11c and e are also aligned along time 0. Therefore, the average velocity is assumed to be 6.44 km/s for all the *PmP* reflection picks from lines 1250, 1255, and 1256, and for part of the main fjord line with midpoints located to the west of the CSZ.

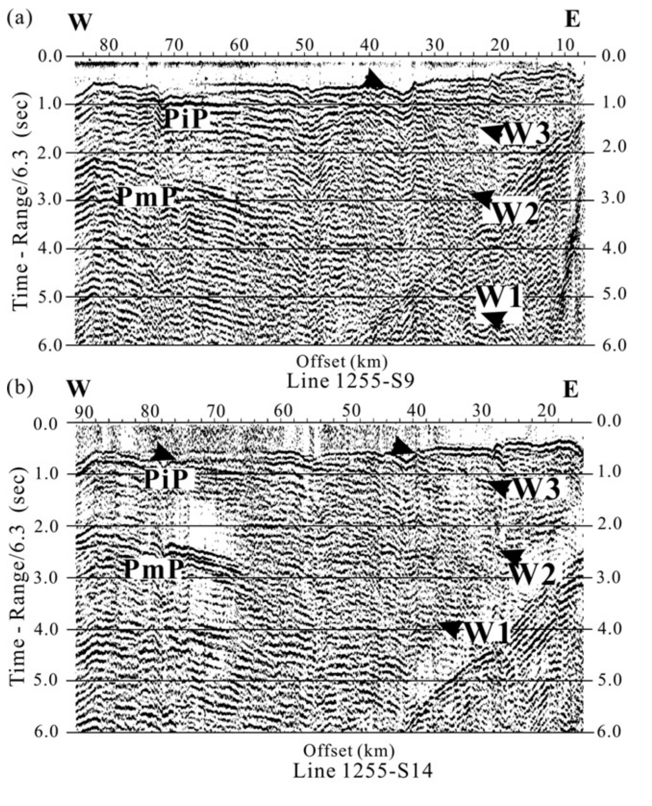

Fig. 10. Vertical-component receiver gathers 9 (a) and 14 (b) from line 1255. Dipping reflections W1, W2, and W3 observed in these records could correspond to reflections from thrust faults interpreted by Morozov et al. (1998). Note that large shot statics are usually present near surface traces of these faults.

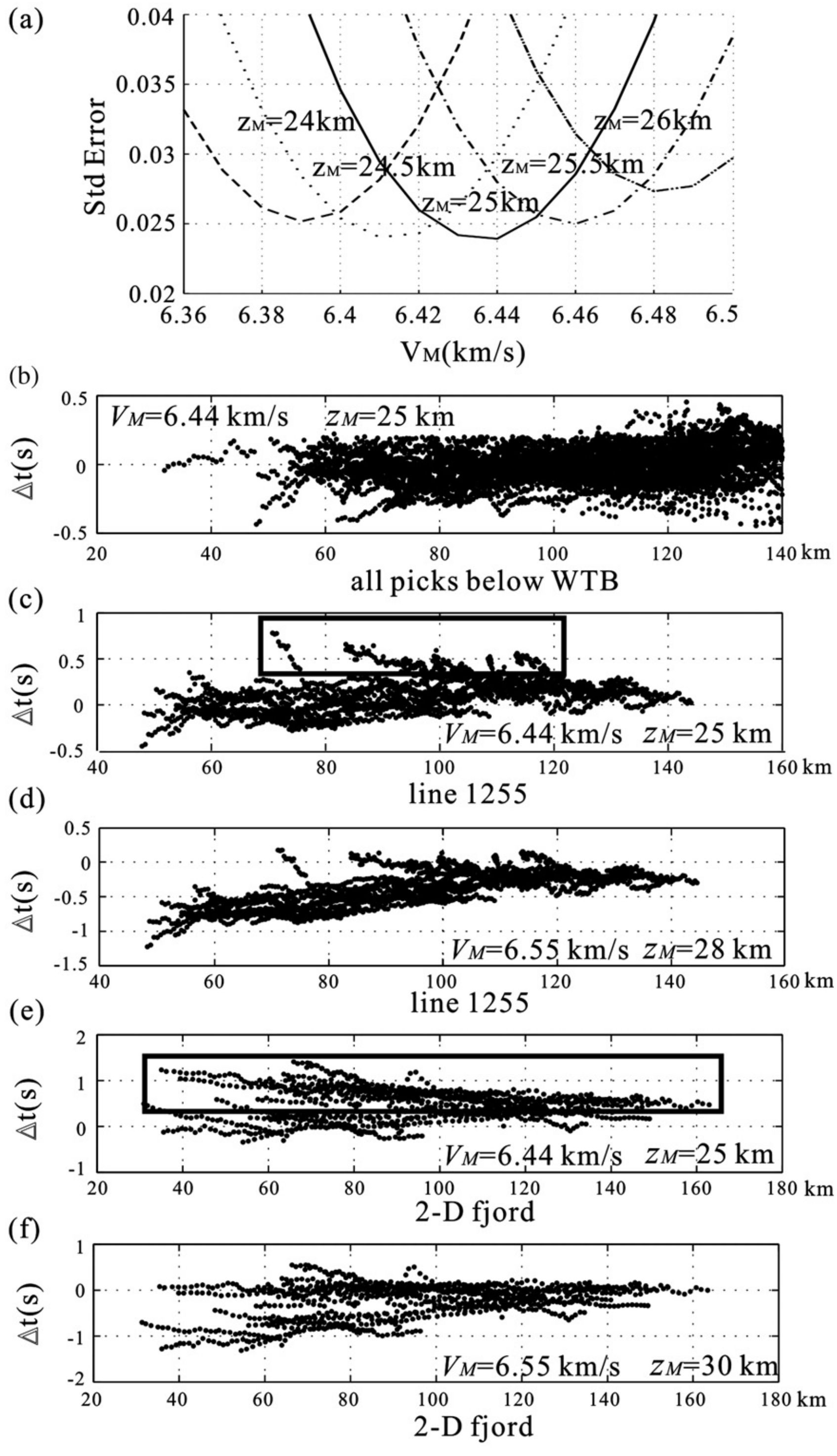

Fig. 11. (a) The standard error of the observed and modeled Moho reflection times below the WTB with different velocity models; (b) Error residuals between the observed Moho and modeled Moho reflection times from all the picks below WTB with an RMS velocity 6.44 km/s and a Moho depth of 25 km; (c) Error residuals from line 1255 with an average velocity 6.44 km/s and a Moho depth of 25 km; (d) Error residuals from line 1255 with an average velocity of 6.55 km/s and a Moho depth of 28 km; (e) Error residuals from the 2-D fjord line with an average velocity of 6.44 km/s and a Moho depth of 25 km; (f) Error residuals from the 2-D fjord line with an average velocity of 6.55 km/s and a Moho depth of 30 km. The anomalous points indicated by rectangular boxes in plots (c) and (e) mainly correspond to the picks with the midpoints located to the east of the CSZ with deeper Moho. Plots (d) and (f) show that these anomalous residuals reduce to ~0 when the average velocity is set to 6.55 km/s with deeper Moho depth.

With conservative estimation of possible travel-time picking errors as due to a single cycle-skipping (~140 ms), the error of the Moho depth would be ~0.5 km. By comparing the Moho depths at the same location determined from different shot lines, the Moho depth errors are usually within ±0.6 km. Moreover, shot statics, which are typically below 200 ms (with the exception of the areas of the Tertiary grabens) also lead to the maximum Moho depth error estimate of ~0.65 km. Therefore,

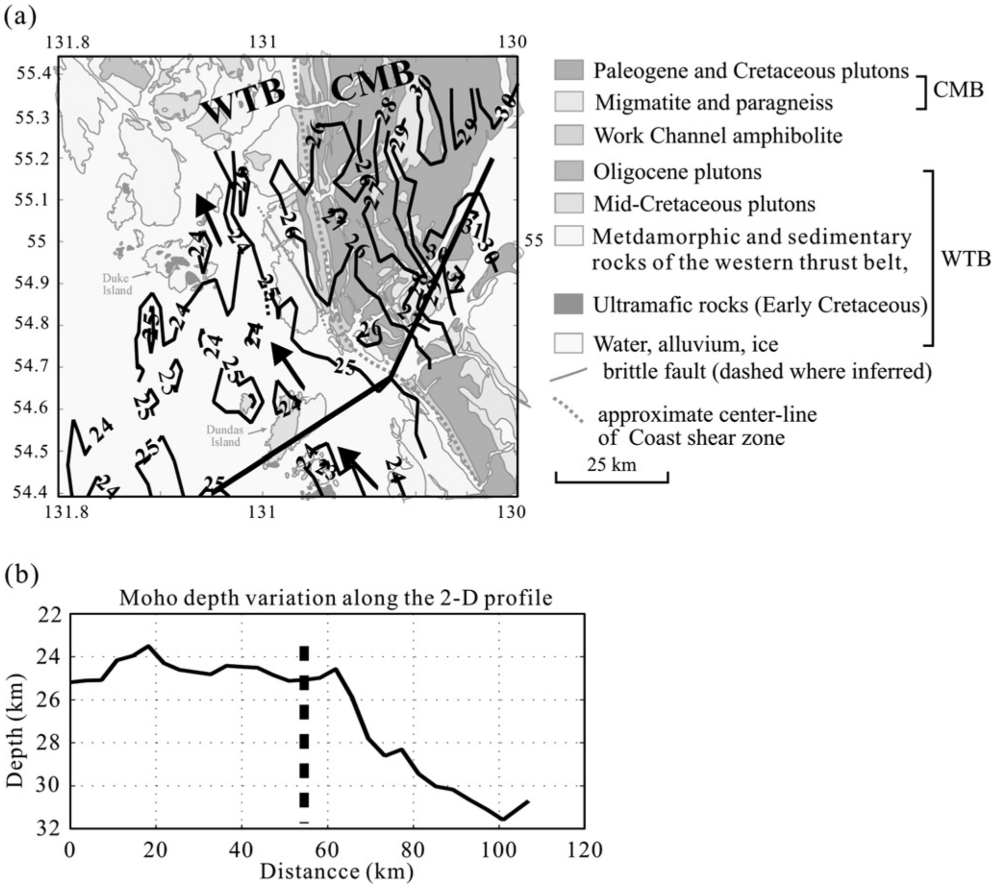

Fig. 12. (a) Moho depth (contours) superimposed on the geologic map (from ACCRETE project website, http://geoweb.princeton.edu/research/ACCRETE/geomap.pdf); (b) 2-D Moho depth variation along the profile shown on (a). Arrows indicate the probable extension direction of the Moho arch. The errors of the Moho depths are generally <2 km.

the maximum total error of the Moho depth from the average velocity model is expected to be <2 km.

As a final result, a contour plot of the resulting Moho depth was superimposed on a geologic map (Fig. 12a). Due to picking quality at far offsets, the Moho picks at offset > 140 km were not used in this figure; therefore, the coverage of this plot does not cover the north part of the midpoints of line 1256 (Fig. 2). To the west of the CSZ, the Moho depth increases gradually over ~100 km distance from ~24 km in the southwest to ~26 km in the northeast. A localized Moho uplift in this area, with a depth of 23–25 km which may also extend northward, is located near the Dundas island. Northeast at the CSZ, the Moho begins to dip steeply from ~26 km to 31 km within a ~15-km long ramp zone, and the contour lines are generally parallel to the exposed CSZ. A Moho cross-section close to the main fjord line (Fig. 12b) was extracted from the 3-D plot, indicating that the 3-D Moho variation derived from the above time-depth conversion is consistent with the previous 2-D interpretation (Morozov et al., 1998, 2001).

5. Discussion

The velocity profile derived to the west of the CSZ is consistent to that obtained along the primary ACCRETE 2-D corridor down Portland Canal (Morozov et al., 1998; Hammer et al., 2000). Along with the regional similarity, the Moho depth contour plot also suggests a ~2 km Moho arch in the vicinity of the Dundas island (Fig. 12a). This feature was also detected by a multi-channel reflection study (J. Diebold and L. Hollister, personal communications, Morozov et al., 1998) and could be attributed to Eocene crustal extension (Hollister and Andronicos, 1997). From the contour plot, this Moho arch also appears to extend northwest (Fig. 12a).

According to Hyndman and Lewis (1999), low seismic velocities (7.8 km/s) and high heat flow (70–120 mW/m^2) across the Intermontane belt of British Columbia correspond to temperatures of about 800–1000 °C at the Moho, based on a low-T dunite velocity of 8.4 km/s and $\frac{\delta v_p}{\delta T}$ of -0.6×10^{-3} km/s/°C. The heat flow at the Portland Canal fjord is also high with an average of 82 mW/m^2 (Sass et al., 1985; Lewis, 1997) and quickly decreases toward the west (Sass et al., 1985; Hyndman and Lewis, 1999) in the coastal area. Therefore, the observed low upper mantle velocities (~7.7–7.9 km/s) below the WTB and the CMB indicate high mantle temperatures (Morozov et al., 1998; Hammer et al., 2000; Morozov et al., 2001, 2003; Hammer and Clowes, 2004). The low upper mantle velocity, together with the observed high heat flow in the CMB and the west of the CSZ suggests a nearly partial melt of the upper mantle (Hammer and

Clowes, 2004), which may be associated with the crustal extension or transtension in the Eocene (Hyndman and Lewis, 1999).

The physical properties of the outboard terranes were further defined by the strong mid-crustal and Moho reflections (Fig. 3) and the high lower crustal velocities. The lower crustal thickness is determined as ~11–14-km thick according to wide-angle refractions and reflections. Given the indications of high lower-crustal temperatures, the velocity of the lower crust (Figs. 8 and 9) would exceed 7 km/s at normal crustal temperatures. According to the previous *S*-wave study (Morozov et al., 2001, 2003), the Vp/Vs ratio of the lower crust below the WTB is high (1.88). Such high *P*-wave velocity and Vp/Vs are appropriate for gabbro (Christensen, 1996). South of the ACCRETE area, seismic studies in the Hecate strait (Yuan and Spence, 1992; Spence and Asudeh, 1993), and the Queen Charlotte Sound (Yuan and Spence, 1992; Spence and Asudeh, 1993) also indicated a 6–10-km thick high-velocity (up to 7 km/s after temperature correction) lower-crustal layer and a crustal thickness under 30 km. Similar observations were also made in the terranes to the west of the San Andreas fault (Howie et al., 1993). Such a consistent high-velocity lower crustal layer is compatible with gabbro, which may result from oceanic or magmatic underplating (Holbrook and Mooney, 1987; Howie et al., 1993).

Mapping the crustal thickness and extension to the west of the 2-D ACCRETE profile along Portland Canal (Fig. 2) was the primary goal of this study. The new model shows that the characteristic Moho profile (~24–26 km with possible extensional arches W-SW of the CSZ, with a ~15-km long ramp to ~31±1 km depths starting below the surface expression of the CSZ; Morozov et al., 1998, 2001) continues within the midpoint coverage of the quasi-3D seismic experiment (Fig. 12). The onset of crustal thickening (as defined by a Moho depth contour of 26 km in Fig. 12a) is nearly coincident with the CSZ within the area of coverage. The depth contours of the Moho appear to follow the surface expression of the CSZ and correspond to the mid-Cretaceous migmatite and paragneiss belt in the CMB (labeled as the Paleogene arc in Fig. 12a). This observation suggests that the transpression that created the surface CMB has affected the entire crust and followed the existing surface trace of the CSZ.

6. Conclusions

A strong mid-crustal reflection and a ~11–14-km thick high-velocity lower-crustal layer (up to 7 km/s after temperature correction) indicate gabbroic composition in the lower crust of the accreted terranes, which may result from oceanic or magmatic underplating. The average velocity of the whole crust below the WTB is constrained as 6.44±0.02 km/s with a depth of ~24–26 km. The generally northeast dipping Moho below the WTB may suggest that the CMB was mainly constructed during dextral oblique transpression. The northwest-directed Moho arch (>2 km) could be attributed to the Eocene crustal extension.

By combining the results from two broadside lines west of the CSZ with the previous detailed work on the main fjord line, this study extended the previous 2-D model of the Moho depth across the CSZ into 3-D. The NE-dipping Moho zone (from ~24–26 km to the west of the CSZ to ~31±1 km below the CMB within a ~15-km long ramp zone, Fig. 12) is generally parallel to the CSZ and extends along strike for >70 km, which also corresponds to the mainly mid-Cretaceous migmatite and paragneiss in the CMB. Such steeply dipping Moho across the CSZ, the subvertical CSZ, the mid-Cretaceous migmatite and paragneiss below the CMB, and the Mid-Cretaceous west-vergent thrust faults below the WTB, support the Mid- to Late-Cretaceous accretion of the Insular terranes along the CSZ.

Acknowledgements

We thank the many participants of ACCRETE project for data acquisition and initial data analysis. L. Hollister initiated the project and provided the geologic map of the ACCRETE study area. Program *rayinvr* by Colin Zelt was used for traveltime inversion. Our work on this project was supported by NSF grants EAR-92-18482, EAR-92-19294, EAR-95-26753, EAR-97-96252, and EAR-95-26531. Processing and interpretation was carried out at the Seismic Computing Laboratory of the University of Wyoming.

References

Chardon, D., Andronicos, C.L., Hollister, L.S., 1999. Large-scale transpressive shear zone patterns and displacements within magmatic arcs: The Coast Plutonic Complex, British Columbia. Tectonics 18, 278–292.

Chen, J., 1998. Seismic wide-angle migration across the Coast Mountains orogen of southeast Alaska and British Columbia. M.S. thesis, University of Wyoming.

Christensen, N.I., 1996. Poisson's ratio and crustal seismology. J. Geophys. Res. 101, 3139–3156.

Clowes, R.M., Gens-Lenartowicz, E., 1985. Upper crustal structure of southern Queen Charlotte Basin from sonobuoy refraction studies (Canada). Can. J. Earth Sci. 22, 1686–1710.

Crawford, M.L., Hollister, L.S., 1982. Contrast of metamorphic and structural histories across the Work Channel lineament, Coast Plutonic Complex, British Columbia (Canada). J. Geophys. Res. 87, 3849–3860.

Crawford, M.L., Hollister, L.S., Woodsworth, G.J., 1987. Crustal deformation and regional metamorphism across a terrane boundary, Coast Plutonic Complex, British Columbia. Tectonics 6, 343–361.

Crawford, M.L., Crawford, W.A., Gehrels, G.W., 2000. Terrane assembly and structural relationships in the eastern Prince Rupert quadrangle, British Columbia. Geol. Soc. Amer. Spec. Pap. 343, 1–22.

Hammer, P.T.C., Clowes, R.M., 2004. Accreted terranes of northwestern British Columbia, Canada: lithospheric velocity structure and tectonics. J. Geophys. Res. 109, B06305. doi:10.1029/2003JB002749.

Hammer, P.T.C., Clowes, R.M., Ellis, R.M., 2000. Crustal structure of NW British Columbia and SE Alaska from seismic wide-angle studies: Coast Plutonic Complex to Stikinia. J. Geophys. Res. 105, 7961–7981.

Holbrook, W.S., Mooney, W.D., 1987. The crustal structure of the axis of the Great Valley, California, from seismic refraction measurements. Tectonophysics 140, 49–63.

Hollister, L.S., Andronicos, C.L., 1997. A candidate for the Baja British Columbia fault system in the Coast Plutonic Complex. GSA Today 7, 1–7.

Howie, J.M., Miller, L.C., Savage, W.U., 1993. Integrated crustal structure across the south central California margin: Santa Lucia escarpment to the San Andreas Fault. J. of Geophys. Res. 98, 8173–8196.

Hyndman, R.D., Lewis, T.J., 1999. Geophysical consequences of the Cordillera-Craton thermal transition in southeastern Canada. Tectonophysics, 306, 397–422.

Klepeis, K.A., Crawford, M.L., Gehrels, G., 1998. Strain field patterns and structural history of the high temperature Coast Shear Zone near Portland Canal, Southeast Alaska and British Columbia. J. Struct. Geol. 20, 883–904.

Lewis, T., 1997. Heat flow studies near the SNORCLE transect. In: Cook, F., Erdrres, P. (Eds.), In-Slave Northern Cordillera Lithospheric Evolution (SNORCLE) Transect and Cordillera Tectonic Workshop Meeting, No. 56. University of British Columbia, pp. 221–222. Lithospheric Report.

McClelland, W.C., Tikoff, B., Manduca, C.A., 2000. Two-phase evolution of accretionary margins: examples from the North American Cordillera. Tectonophysics 326, 37–55.

Morozov, I.B., Smithson, S.B., Hollister, L.S., Diebold, J.B., 1998. Wide-angle seismic imaging across accreted terranes, southeastern Alaska and western British Columbia. Tectonophysics 299, 281–296.

Morozov, I.B., Smithson, S.B., Chen, J., Hollister, L.S., 2001. Generation of new continental crust and terrane accretion in southeastern Alaska and western British Columbia: constraints from *P*- and *S*-wave wide-angle seismic data (ACCRETE). Tectonophysics 341, 49–67.

Morozov, I.B., Christensen, N.I., Smithson, S.B., Hollister, L.S., 2003. Seismic and laboratory constraints on crustal formation in a former continental arc (ACCRETE, southeastern Alaska and western British Columbia. J. Geophys. Res. 108, 16–1–16-9.

Morozov, I.B., Din, M., in press. Use of receiver functions in wide-angle, controlled-source, crustal seismic datasets. Geophys. J. Int.

Rohr, K.M.M., Currie, L., 1997. Queen Charlotte basin and Coast Mountains: paired belts of subsidence and uplift caused by a low-angle normal fault. Geology 25, 819–822.

Rubin, C.M., Saleeby, J.B., 1992. Tectonic history of the eastern edge of the Alexander terrane, southeast Alaska. Tectonics 11, 586–602.

Sass, J.H., Lawver, L.A., Munroe, R.J., 1985. A heat-flow reconnaissance of southeastern Alaska. Can. J. Earth Sci. 22, 416–421.

Spence, G.D., Asudeh, I., 1993. Seismic velocity structure of the Queen Charlotte Basin beneath Hecate Strait. Can. J. Earth Sci. 30, 787–805.

Van Der Heyden, P., 1992. A middle Jurassic to early Tertiary Andean-Sierran Arc model for the Coast Belt of British Columbia. Tectonics 11, 82–97.

Yuan, T., Spence, G.D., 1992. Structure beneath Queen Charlotte Sound from seismic-refraction and gravity interpretations. Can. J. Earth Sci. 29, 1509–1528.

Zelt, C.A., Smith, R.B., 1992. Seismic traveltime inversion for 2-D crustal velocity structure. Geophys. J. Int. 108, 16–34.